Molecular Therapy
Methods & Clinical Development
Original Article

# Manufacture of CD22 CAR T cells following positive versus negative selection results in distinct cytokine secretion profiles and γδ T cell output

Hannah W. Song,[1,6] Mehdi Benzaoui,[2,3,6] Alka Dwivedi,[2,7] Sarah Underwood,[1,7] Lipei Shao,[1] Sooraj Achar,[4] Vesna Posarac,[5] Victoria A. Remley,[1] Michaela Prochazkova,[1] Yihua Cai,[1] Ping Jin,[1] Robert P. Somerville,[1] David F. Stroncek,[1] Grégoire Altan-Bonnet,[4] Nirali N. Shah,[2] Christopher D. Chien,[2] Naomi Taylor,[2,3,8] and Steven L. Highfill[1,8]

[1]Center for Cellular Engineering, Department of Transfusion Medicine, National Institutes of Health, Bethesda, MD, USA; [2]Pediatric Oncology Branch, National Cancer Institute, National Institutes of Health, Bethesda, MD, USA; [3]Institut de Génétique Moléculaire de Montpellier, University of Montpellier, CNRS, Montpellier, France; [4]Laboratory of Integrative Cancer Immunology, NCI, Bethesda, MD, USA; [5]STEMCELL Technologies, Vancouver, Canada

**Chimeric antigen receptor T cells (CART) have demonstrated curative potential for hematological malignancies, but the optimal manufacturing has not yet been determined and may differ across products. The first step, T cell selection, removes contaminating cell types that can potentially suppress T cell expansion and transduction. While positive selection of CD4/CD8 T cells after leukapheresis is often used in clinical trials, it may modulate signaling cascades downstream of these co-receptors; indeed, the addition of a CD4/CD8-positive selection step altered CD22 CART potency and toxicity in patients. While negative selection may avoid this drawback, it is virtually absent from good manufacturing practices. Here, we performed both CD4/CD8-positive and -negative clinical scale selections of mononuclear cell apheresis products and generated CD22 CARTs per our ongoing clinical trial (NCT02315612 NCT02315612). While the selection process did not yield differences in CART expansion or transduction, positively selected CART exhibited a significantly higher *in vitro* interferon-γ and IL-2 secretion but a lower *in vitro* tumor killing rate. Notably, though, CD22 CART generated from both selection protocols efficiently eradicated leukemia in NSG mice, with negatively selected cells exhibiting a significant enrichment in γδ CD22 CART. Thus, our study demonstrates the importance of the initial T cell selection process in clinical CART manufacturing.**

## INTRODUCTION

Chimeric antigen receptor T cell (CART) therapy has shown much promise in the treatment of B cell hematological malignancies and is being further applied to solid tumors,[1–3] autoimmune diseases,[4–6] and regenerative therapies.[7] Though initial studies demonstrated the important potential of CART,[8–10] the parameters affecting the overall effectiveness of this therapy are still being investigated. Multiple clinical studies have highlighted the role of CART manufacturing on patient outcomes. For example, process variations performed at the beginning of the manufacturing process, including T cell selection and activation, can alter the functional properties of the resulting CART.[11,12] To manufacture therapeutically relevant doses of CART, large numbers of T cells with high purity and functionality are generally required. To obtain these numbers of cells, patients undergo mononuclear cell (MNC) apheresis, which then requires additional processing to remove red blood cells and platelets. One of the simplest and most widely used methods to obtain MNCs is density gradient separation (i.e., Ficoll), which has been extensively used as a starting product for CART manufacturing.[13–16] However, residual tumor cells and monocytes can persist in the cultures, potentially leading to manufacturing failures because of attenuated T cell expansion and transduction.[17,18] In addition, while anti-CD3/CD28 paramagnetic beads can be used to simultaneously enrich and activate T cells for streamlined manufacturing,[19,20] this approach can yield variable purities.[11]

Immunomagnetic T cell selection results in the isolation of purified T cells or T cell subsets in both preclinical and clinical settings.[21–23] Indeed, many CART trials incorporate positive selection as a means of obtaining starting material with high T cell purity. Positive selection of T cells for CART manufacturing can be performed with as few as one (CD3) or two antibodies (CD4 and CD8),[3,11,24–26] but binding of these receptors can potentially stimulate the T cells

Received 2 August 2023; accepted 7 December 2023;
https://doi.org/10.1016/j.omtm.2023.101171.

[6]These authors contributed equally

[7]These authors contributed equally

[8]Senior author

**Correspondence:** Naomi Taylor, Pediatric Oncology Branch, National Cancer Institute, National Institutes of Health, Bethesda, MD, USA.
**E-mail:** taylorn4@mail.nih.gov
**Correspondence:** Steven L. Highfill, Center for Cellular Engineering, Department of Transfusion Medicine, National Institutes of Health, Bethesda, MD, USA.
**E-mail:** steven.highfill@nih.gov

prematurely or prevent co-receptor activity.[27] Conversely, negative T cell selection uses multiple antibodies to eliminate non-T cells. While negative selection is known to yield lower purities than positive selection,[28] it has the benefit of leaving the T cells untouched by antibody-labeled beads. As such, negative selection is preferred in most functional preclinical studies, but importantly, it is less amenable for clinical manufacturing because of the quantity and expense of the multiple good manufacturing process (GMP)-grade antibodies required to remove contaminating cell types.

In the context of a CD22 CART trial carried out at the National Institutes of Health (NCT02315612), the addition of a positive CD4/CD8 selection step, which replaced a CD3/CD28 Dynabead enrichment step—with no other changes in manufacturing—was associated with increased potency in patients with B cell acute lymphoblastic leukemia (B-ALL), but also with an augmented toxicity profile.[11] As such, it was of particular interest to evaluate the feasibility of a clinical scale CD22 CART manufacturing protocol based on the engineering of untouched, negatively selected T cells. To this end, we directly compared apheresis products manufactured via positive CD4/CD8 selection with negatively selected T cells selected using clinical scale (i.e., >2 $\times$ $10^9$ starting cells) manufacturing methods. Selected T cells were activated and expanded in closed-system culture bags to generate CD22 CART, using the 9-day expansion protocol employed in our ongoing clinical trial.[11] Although negative T cell selection resulted in a lower purity of the starting product, this method significantly increased CD3 T cell recovery compared with positive T cell selection. Furthermore, CD22 CART generated from both positive and negative selection ($CART^{pos}$ and $CART^{neg}$) exhibited similar expansion, T cell subsets, activation markers, and CAR expression in the final product. Functionally, $CART^{neg}$ cells exhibited lower *in vitro* cytokine production, but were characterized by a more rapid killing rate. Notably, both $CART^{pos}$ and $CART^{neg}$ displayed high *in vivo* cytotoxicity in a humanized leukemia mouse model, with the latter showing enrichment in γδ CART, a population of interest in anti-tumor immunotherapy strategies.

## RESULTS

### Negative selection of apheresis products results in a lower purity and higher recovery of $CD3^+$ T cells

Negative and positive immunomagnetic-based T cell selections (Figure 1A) were performed on thawed MNC apheresis products from five healthy adult donors and one pediatric donor with B-ALL, with the initial percentages of $CD3^+$ T cells ranging from 20.8% to 57.9% (Figure 1B). T cell purity was higher after positive selection as compared with negative selection (84.0% ± 7.8% vs. 77.5% ± 10.0% $CD3^+$, respectively; $p < 0.05$). In contrast, the recovery of $CD3^+$ T cells was improved by an average of 20% after negative selection (72.7% ± 9.0% vs. 52.6% ± 6.0%, respectively; $p < 0.05$) (Figure 1B), with similar viabilities (87%–96%) (Figure 1B). The most abundant non-$CD3^+$ cell type present after both positive and negative selection was $CD14^+/CD16^+$ monocytes, comprising approximately 10% of total cells in both selected products (Figures 1C and 1D). Interestingly, a 2-fold increase in the antibody cocktail used for negative selection resulted in a higher elimination of the $CD14^+/CD16^+$ monocyte population (Figure 1C, HD4, HD5, Pt), suggesting a non-saturating level of negative-selecting antibodies in the initial selections (Figures 1C and 1D). $CD56^+$ natural killer cells were present at only minimal levels in both selections (0.6% ± 0.4% vs. 1.9% ± 1.3%) while $CD19^+$ B cell contamination trended to higher levels after negative selection (6.2% ± 5.6% vs. 0.3% ± 0.5%) (Figure 1D). Overall, both positive and negative selection methods resulted in the successful isolation of T cells, albeit with differences in both purity and recovery.

### CD22 CART cells generated after positive and negative T cell selection exhibit similar phenotypes and gene expression profiles

After selection, T cells were activated with anti-CD3/CD28 Dynabeads in the presence of interleukin 2 (IL-2). T cells were transduced with clinical-grade lentivirus encoding CD22 CAR[29] and expanded for 9 days as per the clinical manufacturing protocol (Figure 2A).[11] T cells ($30 \times 10^6$) were transduced on day 2, yielding more than $600 \times 10^6$ cells on day 9 (Figure 2B), corresponding with an average 38-fold expansion following both positive and negative selection (Figure 2C). Despite differences in T cell purity immediately after selection, cultures from both positive and negative selection reached 99.4% or greater $CD3^+$ purity by day 9 (Figure 2D). The CD4:CD8 T cell ratio differed substantially between donors, but was not statistically different between $CART^{pos}$ and $CART^{neg}$ at any of the time points, whether gating on $CD3^+$ T cells or transduced only (Figures 2Ei and S1). Of note, CD22CAR transduction, measured as a function of protein L staining, was similar between groups on days 4, 7, and 9, increasing to more than 35% by day 9 (Figure 2Eii). Thus, the T cell selection method did not affect the potential for efficient lentiviral transduction.

To determine whether the T cells were differentially activated during the expansion phase, we monitored the cell surface expression of CD25 and PD1 activation markers via flow cytometry. Nearly identical expression patterns of CD25 were detected on $CART^{pos}$ and $CART^{neg}$; CD25 levels increased from 32% on day 0 to 99% or greater on day 4 before decreasing to approximately 80% positive on day 9 (Figures 2Eiii and S2A). Similarly, PD1 expression increased from approximately 40% on day 0 to 100% positive on day 4, before decreasing to 60% on days 7–9, again with no difference between $CART^{pos}$ and $CART^{neg}$ (Figures 2Eiv and S2A). T cell subsets, including naive/stem cell memory-like ($T_{n/scm}$), central memory ($T_{cm}$), effector memory ($T_{em}$), and terminal effector ($T_{eff}$), were monitored as $CD45RA^+CCR7^+$, $CD45RA^-CCR7^+$, $CD45RA^-CCR7^-$, and $CD45RA^+CCR7^-$, respectively. The distribution of these subsets was similar in both groups, with $T_{n/scm}$ and $T_{eff}$ population comprising the largest subsets, irrespective of whether total T cell or $CAR^+$ populations were evaluated (Figures 2F, S2B, and S2C). Thus, the phenotype of CART cells generated via positive and negative selection seemed to be largely similar.

To further probe potential differences in T cells during the expansion period, transcriptional profiling of a panel of 780 CART-related genes was performed. Principal component analysis (PCA) of gene

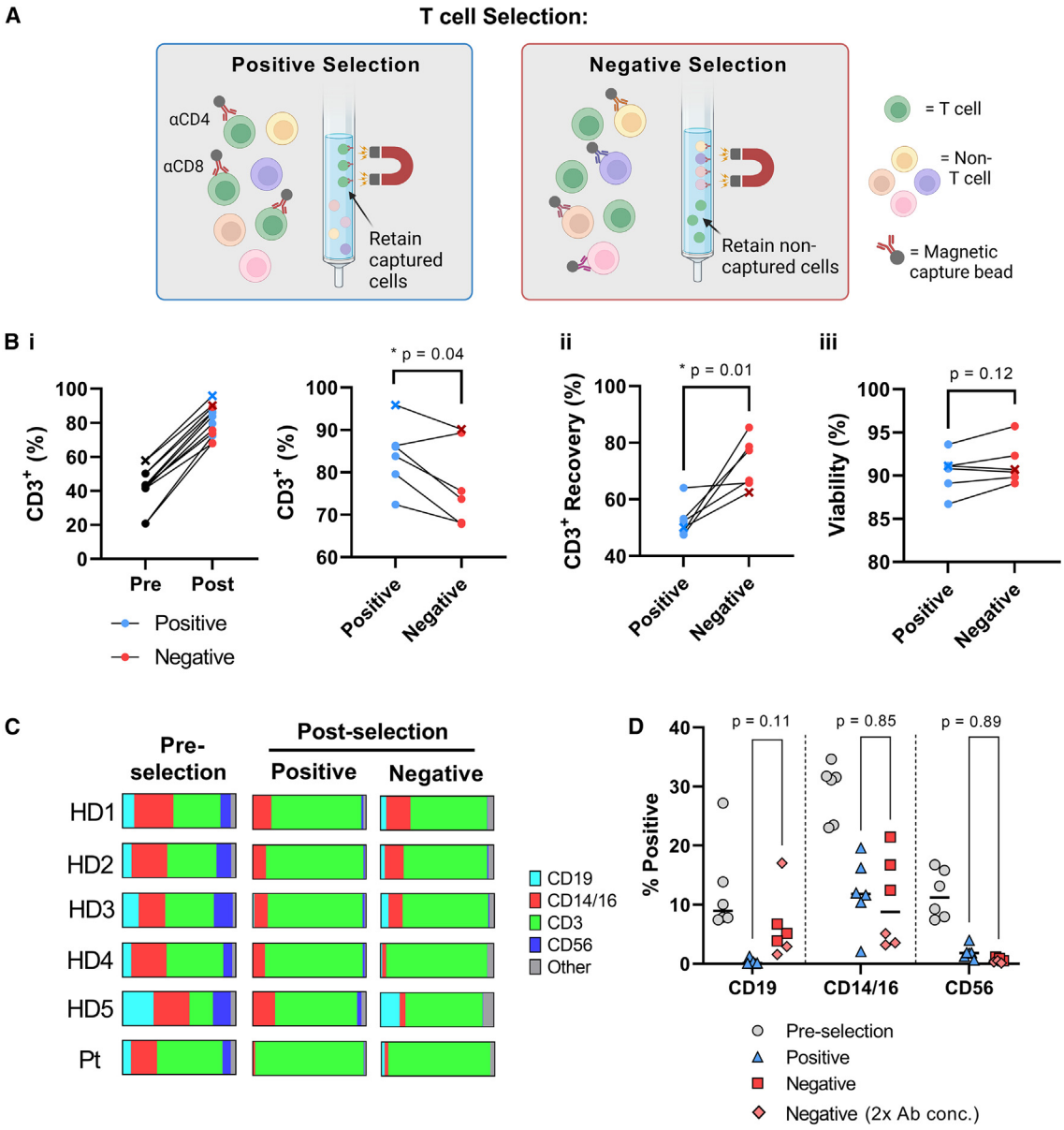


**Figure 1. T cell selection using positive vs. negative selection**

(A) Schematic of selection methods compared in this study; positive selection (anti-CD4 and anti-CD8 immunomagnetic beads) and negative selection (immunomagnetic beads targeting non-T cell subsets). Image created with biorender.com. (B) Different parameters were used to evaluate T cells obtained by positive and negative selection: (i) Purity of $CD3^+$ cells; (ii) recovery of $CD3^+$ cells calculated as the number of $CD3^+$ T cells obtained after selection normalized to input $CD3^+$ cells; and (iii) viability, measured via propidium iodide and acridine orange (AO/PI) staining immediately after selection. The B-ALL patient sample is indicated by an x. (C and D) Flow cytometry was performed on individual samples before and after selection using anti-CD19, anti-CD14/CD16, anti-CD3, and anti-CD56 monoclonal antibodies (mAbs), to distinguish B, monocyte, T, and natural killer cells, respectively. Quantifications are presented for each donor (C) as well as for each subset (D). The antibody concentrations used for negative selection were increased by 2-fold for healthy donor (HD) 4, HD5, and the patient (Pt) as compared with HD1, HD2, and HD3. *$p < 0.05$ using paired t test.

expression levels at days 0, 2, 4, 7, and 9 of culture revealed distinct clustering, but these were based on the kinetics of activation rather than positive vs. negative selection (Figure 2G). Analyses of these signatures revealed a decrease in cytotoxicity and chemokine signaling signatures at later phases of the expansion period (Figure 2H). Interestingly, chemokine signaling was more highly induced in $CART^{neg}$ than $CART^{pos}$ at day 4 (Figure 2H). Activation and exhaustion gene signatures increased during the 9-day expansion phase, but there were no significant differences as a function of the selection method (Figure S3).

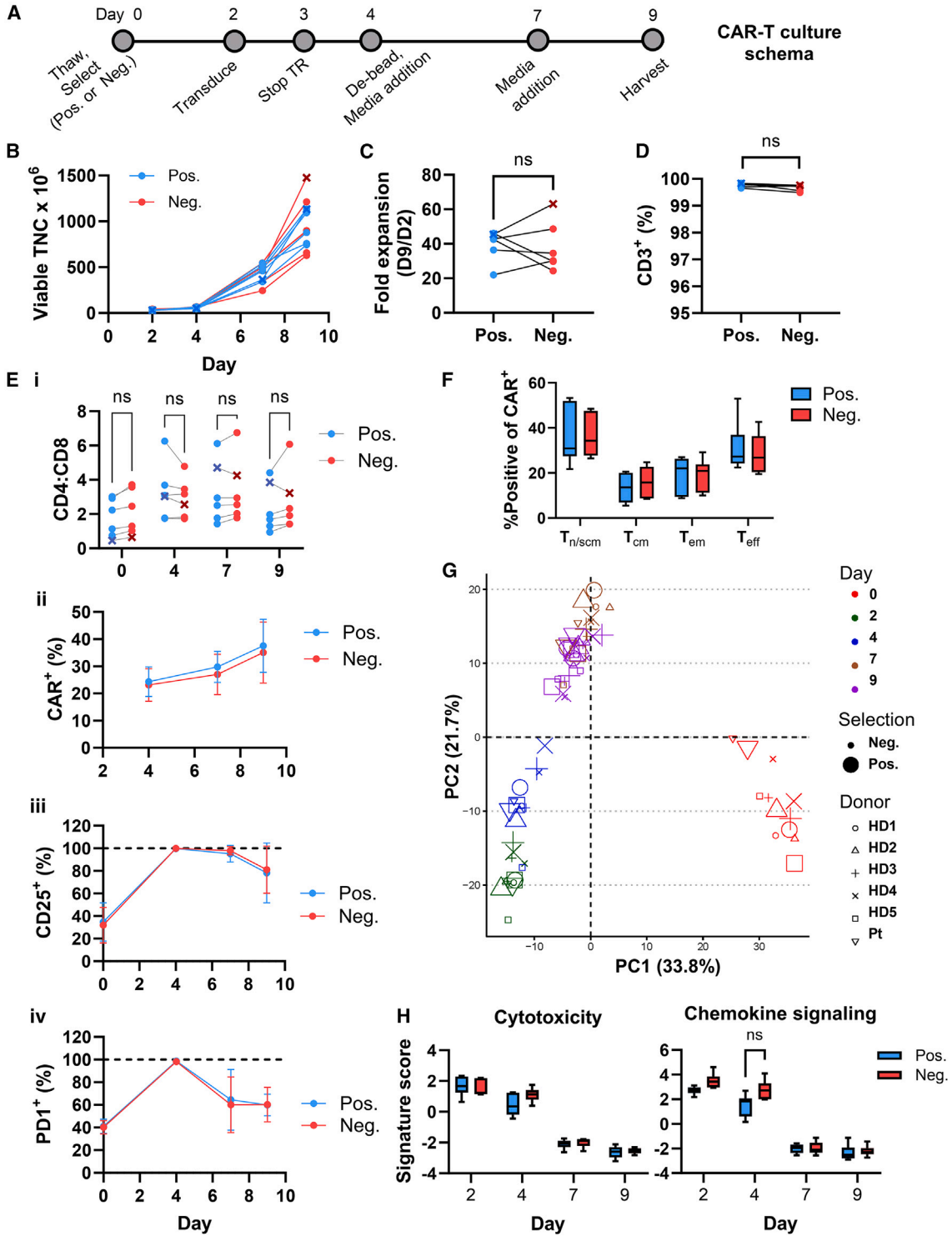


**Figure 2. Generation of CD22 CART from positively and negatively selected T cells**

(A) Schema of the manufacturing protocol used to generate CD22 CART. TR, transduction. (B) Viable total nucleated cells (TNC) are shown between days 2 and 9 of culture. The B-ALL patient sample is indicated with an x. (C) Fold expansion was calculated as TNC on day 9 normalized to TNC on day 2. Lines are used to connect data points from the same donor. (D) $CD3^+$ T cell purity was assessed on day 9 after gating on viable cells. (E) (i) The ratio of CD4:CD8 cells was assessed after gating on viable cells. (ii) Transduction was measured as a function of protein L staining on viable $CD3^+$ cells, plotted as the mean ± SD of six donors. (iii) $\%CD25^+$ T cells was assessed on viable $CD3^+$

*(legend continued on next page)*

### CART$^{neg}$ produce lower levels of cytokines in response to CD22$^{+}$ leukemia, but exhibit a more rapid *ex vivo* killing rate compared with CART$^{pos}$

We further characterized the differentially selected CD22 CART products by evaluating their ability to produce interferon γ (IFNγ), IL-17A, tumor necrosis factor α, IL-2, IL-4, IL-10, IL-6, IL-8, RANTES, MIG, IP-10, and MCP-1 after *ex vivo* stimulation by CD22$^{+}$ NALM6 leukemia at an effector-to-target (E:T) ratio of 1:1. Both CART$^{pos}$ and CART$^{neg}$ produced high levels of cytokines after co-culture with CD22$^{+}$ NALM6 leukemia, at levels significantly elevated as compared with co-culture with CD22$^{-}$ leukemia (Figure 3A). Interestingly, though, IFNγ, IL-2, IL-8, and RANTES were secreted at significantly higher levels by CART$^{pos}$ than CART$^{neg}$ (Figure 3A). To better understand the influence of positive and negative selection on CD22 CART antileukemic activity, a PCA was performed based on the cytokine secretion profiles obtained following leukemia co-culture (Figures S4A–S4C). By determining PCA distances between CART$^{pos}$ and CART$^{neg}$ manufactured from each donor, considerable heterogeneity between donors was detected (Figures S4E and S4F), showing a differential impact of positive and negative selection on the cytokine secretion of CART generated from different donors.

We next assessed the *ex vivo* cytotoxicity of CART$^{pos}$ and CART$^{neg}$ against CD22$^{+}$ leukemia (Figure 3B). CART generated by either method did not kill CD22-negative NALM6, but exhibited potent cytotoxicity against CD22$^{+}$ leukemia. Unexpectedly, though, CART$^{neg}$ exhibited a significantly higher rate of killing than CART$^{pos}$ (Figure 3B), pointing to differences in the regulation of cytokine secretion and anti-tumor cytotoxicity by CD22 CART.

### CART$^{neg}$ and CART$^{pos}$ exhibit similar *in vivo* efficacy against B-ALL

As CART$^{neg}$ and CART$^{pos}$ exhibited high *in vitro* cytotoxicity, we tested the ability of these CART products to eradicate NALM6 *in vivo*. CART$^{pos}$ and CART$^{neg}$ manufactured from two healthy donors and one patient with B-ALL were adoptively transferred into NSG mice 4 days after inoculation of luciferase-expressing NALM6 ($1 \times 10^6$). A limiting dose of CART ($3 \times 10^6$), where relapse is expected, was used to potentially discriminate between potential functional differences between CART$^{pos}$ and CART$^{neg}$. Interestingly, the *in vivo* efficacy of CART products varied significantly between donors, with mice adoptively transferred with CD22 CART from HD3 relapsing more rapidly than mice receiving CD22 CART products from healthy donor 4 or a patient, irrespective of the selection method (Figures 4A and 4B). There was no significant difference in leukemia growth or overall survival of NSG mice adoptively transferred with CART$^{pos}$ or CART$^{neg}$, although intriguingly, CART$^{neg}$ generated from the patient had lower overall disease burden at day 48 as compared with CART$^{pos}$. Moreover, consistent with the high donor-to-donor variability, the phenotype of T cells persisting in the spleens and bone marrow of these mice exhibited high variability; the percentages of PD1$^{+}$CD39$^{+}$ T cells, a phenotype of T cell exhaustion, as well as CD4:CD8 ratios varied markedly in mice treated with CD22 CART from the different donors (Figure S5). Thus, variability, even between healthy donors, resulted in significant differences in the ability of CD22 CART to control *in vivo* leukemic growth.

### CD22 CART generated from negatively selected T cells include CD22 CAR$^{+}$ γδ T cells

As *in vivo* leukemia eradication experiments demonstrated high donor-to-donor variability, transcriptional profiling analysis was used to assess potential donor-independent differences between CART$^{neg}$ and CART$^{pos}$. Interestingly, only 9 of 780 genes were differentially expressed in CART$^{neg}$ and CART$^{pos}$ at the end of the expansion phase (day 9, $p < 0.05$) (Figure 5A). Of these nine genes, only two, *TRDC* and *TRDV2*, were differentially expressed on day 7 as well as day 9, both upregulated in CART$^{neg}$ as compared with CART$^{pos}$ (Figures 5A and S6). *TRDC* and *TRDV2* are specifically expressed on γδ T cells, encoding the T cell receptor delta chain. Therefore, we investigated whether γδ T cells were present at different levels in CART$^{neg}$ and CART$^{pos}$.

As expected, αβ T cells made up the vast majority of T cells in the final products,[30] accounting for at least 97% of total cells on day 9 of culture (Figure 5B). Notably, though, there was a 4.4-fold higher level of αβ$^{neg}$ cells in negatively selected as compared with positively selected T cells (0.9% ± 0.8% vs. 0.2% ± 0.2%; $p < 0.001$) (Figure 5B). Consistent with the gene expression data, a 6-fold higher level of αβ$^{neg}$ cells were γδ T cells, identified as Vδ1$^{+}$ or Vδ2$^{+}$ ($p < 0.001$) (Figure 5C), with Vδ2 encoded by the *TRDV2* gene (Figure 5A). Importantly, the Vδ1$^{+}$ and Vδ2$^{+}$ subsets corresponded with cells in the CD4$^{-}$CD8$^{-}$ compartment (Figure 5D). It was interesting to note that αβ T cells were overall transduced at higher levels (37.4% ± 3.3% vs. 35.9% ± 4.0% for positive and negative selection, respectively) than γδ T cells ($p = 0.02$ and 0.006), but the percentage transduction for γδ T cells isolated by the two separation methods were similar (17.1% ± 5.1% vs. 19.5% ± 5.8%) (Figure 5E). Nonetheless, because the initial frequencies of γδ T cells were significantly higher in the negatively selected samples (Figure 5B), this resulted in 4.6-fold higher percentage of γδ T cells in the transduced cells within the negatively selected subset (1.0% ± 0.6% vs. 0.2% ± 0.2%; $p = 0.002$) (Figure 5F). Furthermore, this translated to a significantly higher frequency of γδ T cells within the CAR-transduced CD4$^{-}$CD8$^{-}$ compartment, increasing from 11.3% ± 4.8% to 30.5% ± 5.0% in the negatively selected population

cells, plotted as the mean ± SD of six donors. (iv) PD1 expression was assessed on viable CD3$^{+}$ cells and means ± SDs of PD1$^{+}$ T cells from the six donors at days 2–9 are presented. (F) Naive/stem/central memory-like ($T_{n/scm\text{-}like}$), central memory ($T_{cm}$), effector memory ($T_{em}$), and terminal effector ($T_{eff}$) T cells were monitored by flow cytometry as CCR7$^{+}$CD45RA$^{+}$, CCR7$^{+}$CD45RA$^{-}$, CCR7$^{-}$CD45RA$^{-}$, and CCR7$^{-}$CD45RA$^{+}$, respectively and gated from the CD3$^{+}$CAR$^{+}$ population. Day 9 means ± SEM (n = 6) are shown. (G) PCA and (H) pathway analysis of gene expression data assessed at days 2, 4, 7, and 9 of culture. Means ± SEM for the six donors are shown. Statistical significance was calculated using a multiple paired t test; ns > 0.05.

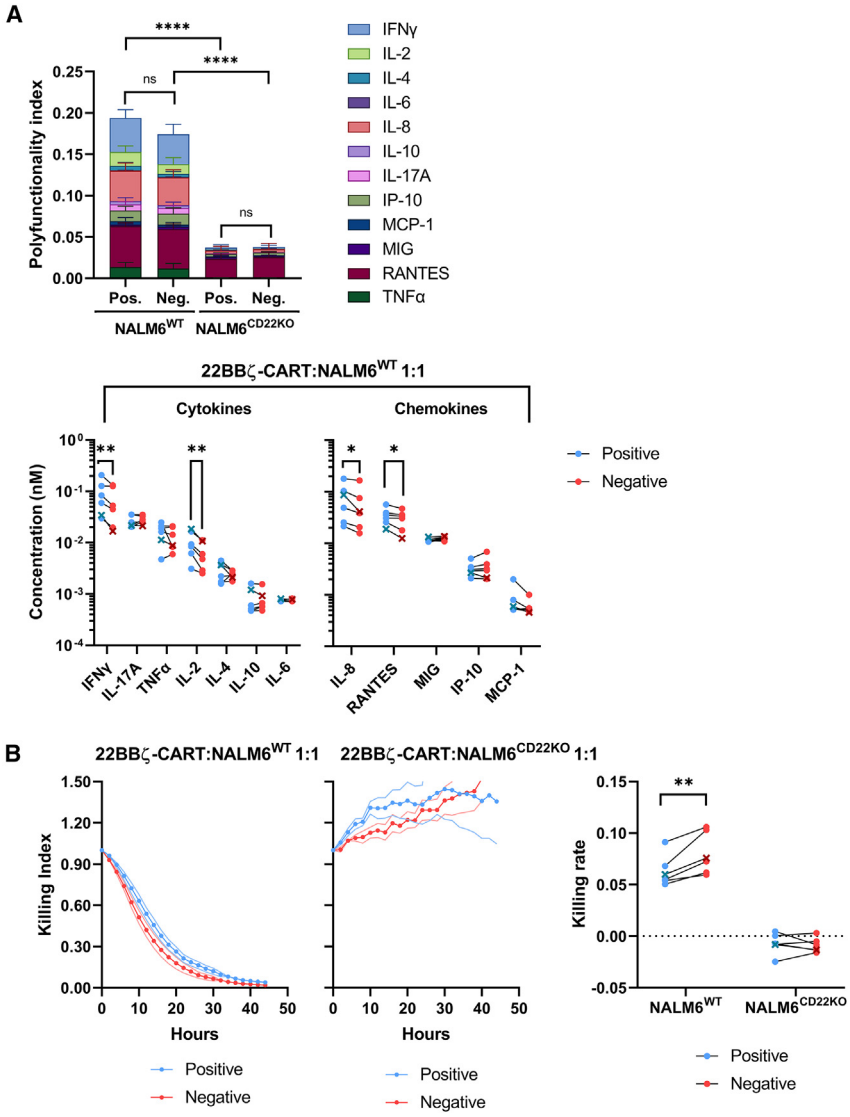


**Figure 3. CD22 CART$^{pos}$ and CART$^{neg}$ eradicate NALM6 leukemia *in vitro***

(A) Production of IFNγ, IL-17A, tumor necrosis factor α (TNFα), IL-2, IL-4, IL-10, and IL-6 cytokines and IL-8, RANTES, MIG, IP-10, and MCP-1 chemokines by CD22 CART$^{pos}$ and CART$^{neg}$ were monitored over 72 h following co-culture with CD22$^{+}$ or CD22$^{-}$ (CD22$^{KO}$) NALM6. Average cytokine concentrations were min/max scaled by the lower and upper detection limits of each cytokine across all samples and divided by the number of cytokines to yield a polyfunctionality index, presented as an average of six individual donors (top). Cumulative concentrations of each cytokine and chemokine are presented (bottom). The ALL patient sample is indicated with an x. (B) *In vitro* anti-leukemic activity of CD22 CART$^{pos}$ and CART$^{neg}$ were monitored against NALM6$^{WT}$ and NALM6$^{CD22KO}$ at a 1:1 effector/target ratio, evaluated as a function of GFP expression. Killing indices (left) and killing rates (right) from six individual donors are presented. Statistical significance was calculated using ratio paired t tests; *p < 0.05, **p < 0.01, ****p<0.0001.

($p < 0.05$) (Figure 5F). The higher percentage of γδ T cells was not specific to the negative T cell selection performed here, as γδ T cells were also recovered at higher frequencies when lymphocytes were selected by both positive CD3/CD28 enrichment (3.2% ± 0.03%) and a non-GMP negative enrichment (1.8% ± 0.06%, EasySep). These data demonstrate the potential for diverse T cell isolation processes to recover γδ T cells in the selected product (Figure 5G). Thus, T cell selection––either via a clinical scale negative selection or a CD3/CD28 enrichment––but not via a CD4/CD8 T cell selection, allows for an enrichment of γδ T cells in the final expanded product, and these cells are successfully transduced by the CD22 CAR vector (Figure 5H).

## DISCUSSION

Given the impressive success of CARTs in the treatment of hematological malignancies, there are an expanding number of tools and reagents available for clinical-grade CART manufacturing. As such, investigators can better tailor their manufacturing methods to suit their desired product characteristics.[15] Our group, as well as others, have found that T cell selection is a key step in the success of CART manufacturing[11,17,31,32]; it defines the subsets of cells that are present, or absent, both in the initial culture as well as in the final infusion product. The positive selection of T cells, based on their binding to anti-CD4 and anti-CD8 monoclonal antibodies, has become a commonly used method in both hematological and solid tumor CART applications, leading to robust manufacturing.[3,11,24,25]

Our ongoing CD22 CART clinical trial demonstrated that switching from a CD3/CD28 enrichment to a CD4/CD8-positive selection improved the reproducibility of CART manufacturing. Interestingly, this change led to a greater efficacy of the CD22 CART but also to an increased incidence of hemophagocytic lymphohistiocytosis (HLH)-like toxicity. The toxicity resulted in a dose de-escalation from $1 \times 10^6$/kg to $3 \times 10^5$/kg; while this dose had been ineffective in the initial manufacturing, it was effective after implementation of the positive selection step.[11] These data led us to hypothesize that CD4/CD8-positive selection may impact the functional characteristics of CART cells, either by modulating signaling through CD4/CD8, by enriching for T cell subsets with different functional properties, and/or by the impact of non-T cell subsets in the initial culture. Indeed, previous studies have shown that CD4/CD8 binding alters cytokines including IL-4,[33] and binding of CD4 selection beads increases mitogen-activated protein kinase signaling.[27]

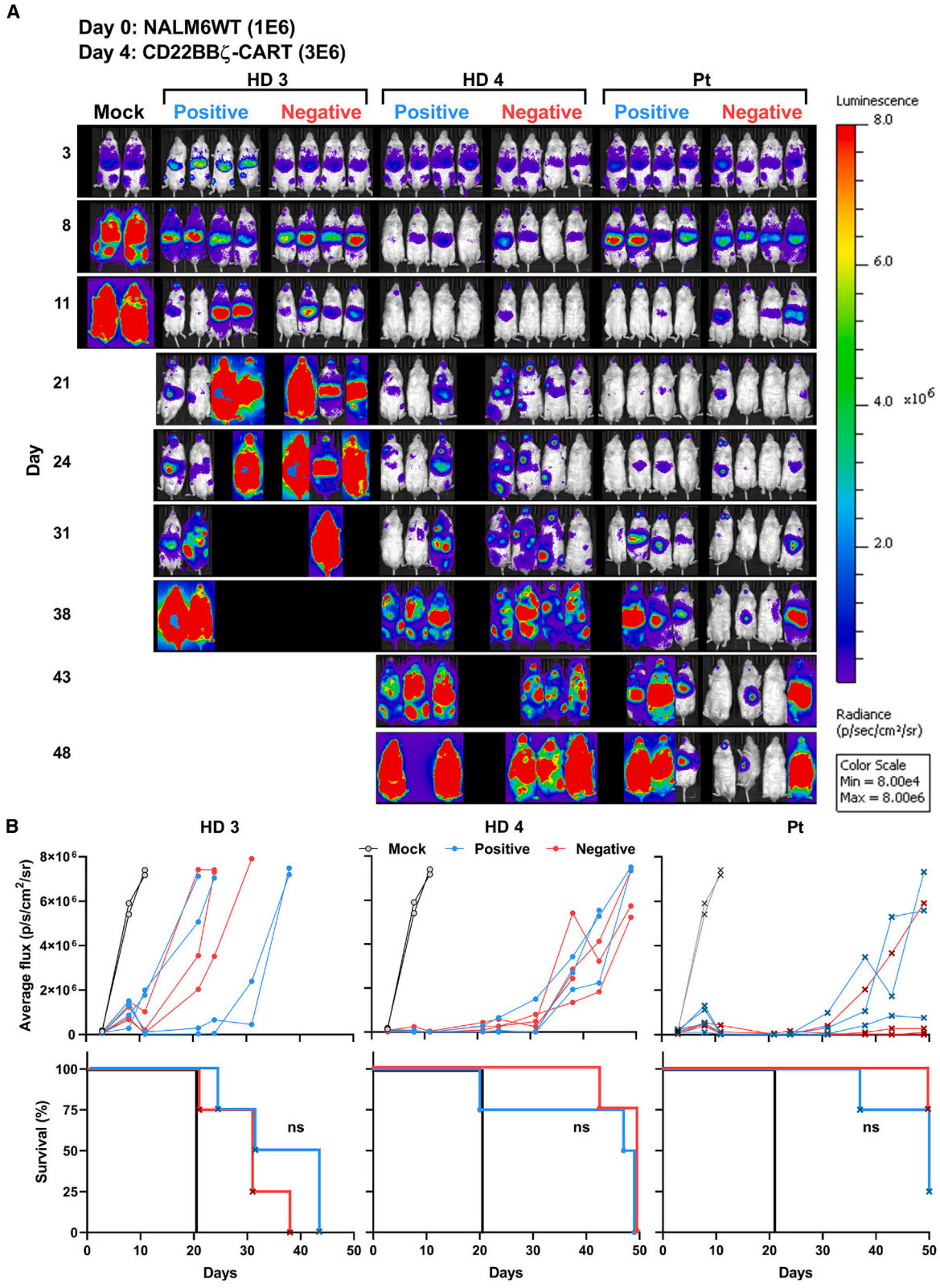


*(legend on next page)*

Here we tested whether purification of unmanipulated T cells after a negative selection protocol using the RoboSep-C platform would alter the functional properties of CD22 CART and compared these cells to CD4/CD8 selection via CliniMACS Plus. Negative T cell selection resulted in a CD22 CART final product with similar expansion, transduction efficiency, and phenotype compared with CD4/CD8 positive selection. Notably, though, differences in cytokine secretion and *in vivo* anti-tumor responses revealed important donor-to-donor variability, outweighing changes in the selection protocol. Indeed, very recent work has shown that the level of stimulation used during the generation of CART should be tailored to individual differences in the donor cells.[34] That being said, the selection protocol did result in some significant differences; positive selection was associated with higher levels of several proinflammatory cytokines such as IFNγ and IL-8. High levels of IFNγ have previously been associated with multiple systemic toxicities, most notably as a marker of cytokine release syndrome,[35–37] as well as HLH-like toxicities in patients receiving CD22 CART[11] and CD19 CART.[38] Thus, negative T cell selection might translate into decreased HLH incidence or severity of inflammatory toxicities.

Because the majority of γδ T cells lack both CD4 and CD8 receptors, CD4/CD8-positive selection significantly reduced the numbers of these immune effectors in the final product, compared with both our negative selection protocol using the RoboSep-C platform as well as to T cells positively enriched using CD3/CD28 Dynabeads. While comprising only 1%–5% of the T cells in the circulation,[30] γδ T cells are primed for rapid toxicity against both foreign antigens and tumor cells. Strikingly, a pan-cancer gene expression analysis revealed that intratumoral γδ T cells are strongly associated with a favorable prognosis.[39] Although non-transduced γδ T cells naturally exert anti-tumor function, transduction of γδ T cells with a CAR may direct their cytotoxicity toward tumor targets while retaining their ability to present antigen, resist exhaustion, and home to the tumor microenvironment.[40] It will be important to elucidate the *ex vivo* expansion conditions that allow for an optimal transduction of γδ T cells, as our data show that the expansion conditions used here resulted in a significantly higher transduction efficiency of αβ as compared with γδ T cells. This is especially pertinent as a longitudinal analysis of CD19 CART in a CLL patient who achieved a durable complete response revealed the expansion of a γδ T cell population, accounting for up to 33% of all $CAR^+$ cells by 3 months after infusion. This context was associated with the emergence of a proliferative CD4 CART population that persisted over a decade,[41] suggesting that γδ CART can contribute to both the initial and later phases of tumor elimination. Long-term studies in appropriate animal models with cross-reactive immune cells and cytokines, supporting human CART survival and persistence, are therefore needed to specifically study the role of γδ CART and its interplay with αβ CART. Given the high level of *in vivo* expansion capability, even limited numbers of γδ CART cells may favorably impact patient outcomes.

In conclusion, our study demonstrates that negative T cell selection is a viable manufacturing strategy that may improve therapeutic outcomes, particularly in certain donors, and should be tested clinically. We find that negative selection reduces cytokine production upon tumor re-stimulation while also increasing γδ CART output, potentially reducing the severity of inflammatory toxicities and improving tumor eradication.

## MATERIALS AND METHODS

### Cell selection

Cryopreserved MNC apheresis products from five healthy donors and one pediatric B-ALL patient were thawed and washed once in Plasmalyte A (Baxter) + 0.5% human serum albumin (HSA) (Baxalta) and split to perform positive and negative T cell selections in parallel; between 2.5 and 3.3 × $10^9$ MNCs were selected in each process. Of note, cryopreserved MNC products have been found to be equivalent to their freshly isolated counterparts as regards expansion, CAR transduction, and patient responses.[42,43] Positive T cell selection was performed using CliniMACS Plus (Miltenyi Biotec) with anti-CD4 and anti-CD8 GMP magnetic selection beads (Miltenyi Biotec) for a combined CD4/CD8 selection. Briefly, thawed cells were washed twice with PBS/EDTA + 0.5% HSA to remove platelets, blocked with 1.5 mg/mL intravenous immunoglobulin (Baxter Healthcare) for 5 min and then labeled with magnetic capture beads for 30 min at room temperature. Labeled cells were then washed twice with PBS/EDTA + 0.5% HSA to remove unbound beads before proceeding to automatic selection on the CliniMACS Plus instrument. For negative selection, MNC apheresis products were loaded onto the RoboSep-C instrument (Stem Cell Technologies), for automated antibody/bead labeling and magnetic T cell selection. The instrument performed incubation with a cocktail of seven proprietary antibodies against non-T cell targets followed by incubation with magnetic beads to capture labeled cells. Healthy donors 1, 2, and 3 were selected with one-half the antibody concentration used for healthy donors 4 and 5 and the B-ALL patient sample. All selections were performed in the absence of human serum. For comparisons with CD3/CD28-enriched cells and non-GMP-negative selection, elutriated lymphocytes were enriched using the Dynabead Human T-expander (Gibco) and EasySep T cell isolation kits (Stem Cell Technologies), respectively, according to the manufacturers' recommendations. Cell counts prior to positive and/or negative selection were performed on the Advia 120 (Siemens), while cell counts and viability after T cell selection were performed on the Cellometer instrument using propidium iodide and acridine orange staining (Nexcelom Biosciences).

**Figure 4. Both CD22 $CART^{pos}$ and $CART^{neg}$ exhibit *in vivo* anti-leukemic activity**

(A) On day 0, luciferase$^+$ NALM6 cells (1 × $10^6$) were injected via tail vein into NSG mice, followed by the injection of CD22 $CART^{pos}$ and $CART^{neg}$ (3 × $10^6$) at day 4. Leukemia growth was evaluated over 50 days by bioluminescent imaging and images at the indicated time points are presented. (B) Bioluminescence ±SEM at each time point was quantified and tumor progression in each mouse is shown.

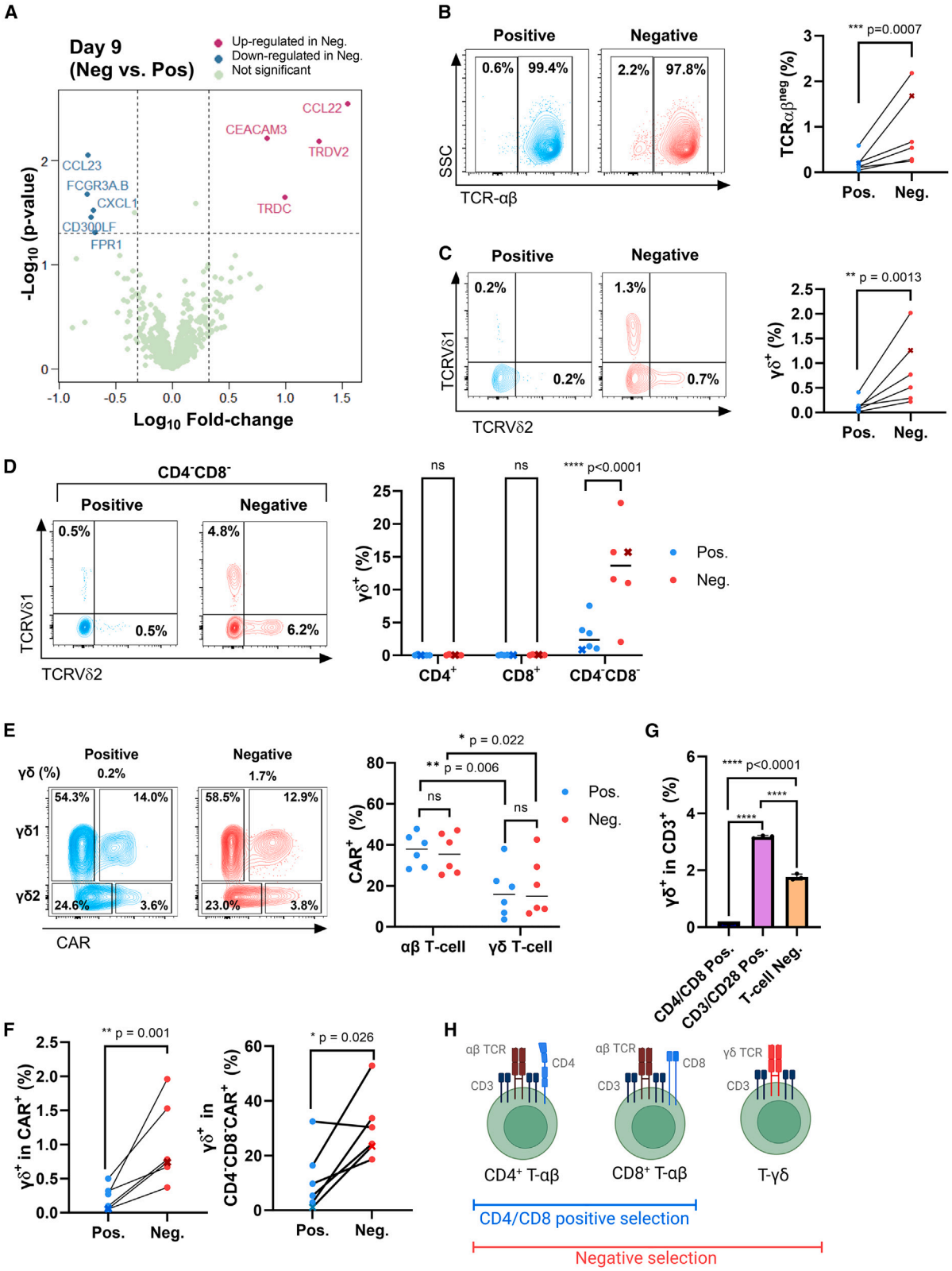


*(legend on next page)*

### CD22 CART generation

T cells enriched via positive and negative selection were placed into culture immediately after selection. Approximately 100 million T cells were activated using Dynabeads (Thermo Fisher Scientific) at a bead to T cell ratio of 3:1 and cultured in bags (Origen Biomedical) at 37°C and 5% $CO_2$. Media on day 0 was composed of AIM-V (Thermo Fisher Scientific) supplemented with 5% human AB serum (Valley Biomedical), 2 mM GlutaMAX (Thermo Fisher Scientific) and 40 IU/mL IL-2 (Clinigen). On day 2, 30 million T cells were transduced for 24 h with 10 μg/mL protamine sulfate (Fresenius Kabi) at a multiplicity of infection of 10 using clinical-grade lentiviral vector encoding CD22 CAR with 41BB and CD3ξ co-stimulatory domains (Lentigen Inc.). Cells were de-beaded on day 4 and diluted to a density of $0.4 \times 10^6$/mL with fresh media containing a higher IL-2 concentration (100 IU/mL). On day 7, cells were diluted again with fresh media to a density of $0.4 \times 10^6$/mL and harvested on day 9. At harvest, cells were washed twice with Plasmalyte A + 0.5% HSA and cryopreserved in Cryostor CS10 (BioLife Solutions) for subsequent downstream analyses.

### Flow cytometry

Cells were resuspended in PBS + 0.5% HSA and stained for 30 min at 4°C. Cells were washed once and analyzed on either a FACSCanto (BD Biosciences) or Cytoflex flow cytometer (Beckman Coulter). Antibodies used for flow cytometry are listed in Table S1.

### Gene expression analysis

Gene expression was measured using the nCounter Analysis Pipeline (NanoString Technologies) with the CART characterization gene panel (n = 780 genes), and data were analyzed using nSolver and R environment. Pathway enrichment was performed using a GSVA package in R with a custom script.

### High-throughput cytokine secretion analysis

CART ($2.5 \times 10^4$) were co-cultured with NALM6 (harboring the GFP and luciferase reporter genes) in 200 μL RPMI media in v-bottom 96-well plates at a 1:1 E:T ratio. The Immunotron robotic platform[44] was programmed to perform automatic collection and replenishment of supernatants at given time points (typically, 1, 3, 6, 12, 18, 24, 30, 36, 42, 48, 60, and 72 h after initiation). Briefly, cell culture plates and medium plates were retrieved from the incubator, 10 μL culture supernatants were collected with minimal disruption of cell pellet and replenished with 10 μL fresh medium. Collected supernatants were stored at −20°C until analysis by cytokine bead array.

### Multiplexed cytokine bead array

Human Th1/Th2/Th17 cytokine and human chemokine bead array kits (BD Biosciences) were used to quantify 7 cytokines and 5 chemokines in each collected supernatant. Collected supernatants were thawed at room temperature, loaded with cytokine bead array (CBA) reagents incubated at room temperature for 15 min. To multiplex acquisition by flow cytometry, plates were then barcoded using fluorescently labeled Fab fragments. Typically, Dy405 or fluorescein isothiocyanate-labeled anti-Rat Fab fragment (Jackson Immunoresearch) were added to a final concentration of 2 μg/mL and incubated for 15 min at room temperature. This reaction was then quenched by adding an excess of Rat IgG (Jackson Immunoresearch) to a final concentration of 30 μg/mL and incubated for 15 min at room temperature. Fab-labeled CBA plates were then consolidated into one plate, washed, and resuspended in fluorescence-activated cell sorting buffer for acquisition on a Fortessa flow cytometer (BD Biosciences).

### Cytotoxicity assay

CARTs ($2.5 \times 10^4$) were co-cultured with NALM6 or NALM6$^{CD22KO}$ at a 1:1 E:T ratio in 200 μL RMPI media in poly-D-lysine-coated (0.05 mg/mL) flat-bottom 96-well plates. Plates were then imaged every 2 h in an S3 IncuCyte live-cell analysis instrument (Sartorius). The killing index was determined as a ratio of the green area at every time point normalized to the first measurement. The killing rate (k) was calculated based on the slope of the natural logarithmic transformation of the killing index curve (y) as a function of time (x) wherein k = –ln(y)/x. After plotting the function ln(y) = –k*x, the ordinate and corresponding abscissa (wherein x > 0) needed to calculate the killing rate were determined using Python.

### *In vivo* analysis of CD22 CART function

The potential for positively and negatively selected CD22 CART to inhibit *in vivo* leukemia growth was assessed in NSG mice as previously described.[24] All animal experiments were conducted under

**Figure 5. Negative selection results in a final CART product enriched in γδ T cells**

(A) Volcano plot representation of differential gene expression between CD22 CART$^{pos}$ and CART$^{neg}$ (day 9). Fold changes of >2 and $p < 0.05$ were considered significant (dotted lines). The identities of several differentially expressed transcripts are indicated. (B) A representative dot plot showing the percentages of TCRαβ$^{neg}$ cells within the viable cell gate is shown for one donor (left). Quantification of TCRαβ$^{neg}$ cells in all donors is shown (right). The B-ALL patient sample is indicated with an "x." (C) T cells expressing TCRVδ1 or TCRVδ2 were monitored by flow cytometry. Representative plots (left) and quantifications (right) are shown. (D) Expression of TCRVδ1 and TCRVδ2 were assessed in CD4$^+$, CD8$^+$, and CD4$^-$CD8$^-$ compartments. A representative TCRVδ1/TCRVδ2 profile in the CD4$^-$CD8$^-$ subset (left) and quantifications (right) are shown. (E) Representative dot plots showing the percentages of CD22 CAR-transduced cells within the TCRVδ1 and TCRVδ2 subsets are shown for one donor (left). Quantifications of the percentages of CD22 CAR-transduced cells within the αβ and γδ populations in the 6 donors, following positive and negative selection, are shown (right). (F) The percentages of γδ (TCRVδ1/TCRVδ2) T cells within the total CAR$^+$ population (left) as well as the percentages of γδ T cells within the CD4$^-$CD8$^-$CAR$^+$ population (right) are presented. (G) T cells were isolated from elutriated lymphocytes using either CD3/CD28 Dynabeads (positive enrichment) or a non-GMP negative T cell selection (EasySep) as compared with CD4/CD8-selected cells. Quantifications of the percentages of γδ T cells within the CD3 populations are indicated (n = 3). (H) Schematic showing that only αβ T cells are retained by CD4/CD8 positive selection whereas γδ T cells are also retained during negative selection (image created with biorender.com). *$p < 0.05$. **$p < 0.01$, ***$p < 0.001$, ratio paired t test (B, C, and F); ns > 0.05, *$p < 0.05$, **$p < 0.01$, two-way ANOVA with multiple comparisons (E); ****$p < 0.0001$, one-way ANOVA with multiple comparison (G).

protocols approved by the National Cancer Institute Institutional Animal Care and Use Committees and in accordance with National Institutes of Health laboratory animal guidelines. Bioluminescent NALM6 ($1 \times 10^6$) were adoptively transferred by tail vein injection at day 0 and CD22 CART ($3 \times 10^6$) were then injected at day 4. Tumor engraftment and growth were assessed by bioluminescent imaging after intraperitoneal injection of D-luciferin (3 mg; Caliper Life Sciences) using the IVIS Lumina Imaging (PerkinElmer). Luminescence was quantified using the RadianceQuantifier Graphical User Interface (available at https://github.com/soorajachar/radianceQuantifier). At study termination, murine bone marrow and spleen were harvested for analysis of leukemia and CD22 CART cells by flow cytometry as described.[24]

### Data and statistical analysis

CBA robotic data were processed as previously described.[44] Briefly, a custom-designed Python pipeline (named Plateypus) was used to simultaneously capture plate-formatted settings, compile high-throughput bulk cytokine/surface marker/single cell data, and perform initial data visualization for quality control (https://doi.org/10.5281/zenodo.5759171). Plateypus is available at https://pypi.org/project/plateypus/. A p value of less than 0.05 was considered significant. Statistical analyses were performed using GraphPad Prism. Images were created using BioRender.

## DATA AND CODE AVAILABILITY

The datasets analyzed in the current study are available from the corresponding authors upon reasonable request.

## SUPPLEMENTAL INFORMATION

Supplemental information can be found online at https://doi.org/10.1016/j.omtm.2023.101171.

## ACKNOWLEDGMENTS

This study was supported by the Center for Cancer Research, Intramural Program, National Cancer Institute (Z99CL999999, ZIABC 011923, and ZIABC011807) and an NCI FLEX award (G.A-B., N.T., and N.N.S.). The views expressed by the authors do not necessarily represent the views of the NIH, Department of Health and Human Services, or the US federal government.

## AUTHOR CONTRIBUTIONS

H.W.S., M.B., C.D.C., N.T., and S.L.H. conceived the study; H.W.S., M.B., A.D., S.U., L.S., S.A., P.J., R.P.S., D.F.S., G. A.-B., N.N.S., C.D.C., N.T., and S.L.H. designed the experiments; H.W.S., M.B., A.D., S.U., L.S., S.A., V.A.R., M.P., and Y.C. performed experiments and V.P. designed and formulated the negative selection antibody cocktail; all authors analyzed and interpreted data; H.W.S., M.B., C.D.C., N.T., and S.L.H. wrote the first version of the manuscript and all authors edited the manuscript; N.T. and S.L.H. supervised the project. All authors approved the final manuscript.

## DECLARATION OF INTERESTS

V.P. is an employee of STEMCELL Technologies, Inc.

## REFERENCES

1. Srour, S., Kotecha, R., Curti, B., Chahoud, J., Drakaki, A., Tang, L., Goyal, L., Prashad, S., Szenes, V., Norwood, K., and Pal, S. (2023). Abstract CT011: A phase 1 multicenter study (TRAVERSE) evaluating the safety and efficacy of ALLO-316 following conditioning regimen in pts with advanced or metastatic clear cell renal cell carcinoma (ccRCC). Cancer Res. *83* (*Supplement*), CT011.
2. Del Bufalo, F., De Angelis, B., Caruana, I., Del Baldo, G., De Ioris, M.A., Serra, A., Mastronuzzi, A., Cefalo, M.G., Pagliara, D., Amicucci, M., et al. (2023). GD2-CART01 for Relapsed or Refractory High-Risk Neuroblastoma. N. Engl. J. Med. *388*, 1284–1295.
3. Majzner, R.G., Ramakrishna, S., Yeom, K.W., Patel, S., Chinnasamy, H., Schultz, L.M., Richards, R.M., Jiang, L., Barsan, V., Mancusi, R., et al. (2022). GD2-CAR T cell therapy for H3K27M-mutated diffuse midline gliomas. Nature *603*, 934–941.
4. Mackensen, A., Müller, F., Mougiakakos, D., Böltz, S., Wilhelm, A., Aigner, M., Völkl, S., Simon, D., Kleyer, A., Munoz, L., et al. (2022). Anti-CD19 CAR T cell therapy for refractory systemic lupus erythematosus. Nat. Med. *28*, 2124–2132.
5. Oh, S., Mao, X., Manfredo-Vieira, S., Lee, J., Patel, D., Choi, E.J., Alvarado, A., Cottman-Thomas, E., Maseda, D., Tsao, P.Y., et al. (2023). Precision targeting of autoantigen-specific B cells in muscle-specific tyrosine kinase myasthenia gravis with chimeric autoantibody receptor T cells. Nat. Biotechnol. *41*, 1229–1238.
6. Lee, J., Lundgren, D.K., Mao, X., Manfredo-Vieira, S., Nunez-Cruz, S., Williams, E.F., Assenmacher, C.A., Radaelli, E., Oh, S., Wang, B., et al. (2020). Antigen-specific B cell depletion for precision therapy of mucosal pemphigus vulgaris. J. Clin. Invest. *130*, 6317–6324.
7. Rurik, J.G., Tombácz, I., Yadegari, A., Méndez Fernández, P.O., Shewale, S.V., Li, L., Kimura, T., Soliman, O.Y., Papp, T.E., Tam, Y.K., et al. (2022). CAR T cells produced in vivo to treat cardiac injury. Science *375*, 91–96.
8. Kochenderfer, J.N., Dudley, M.E., Kassim, S.H., Somerville, R.P.T., Carpenter, R.O., Stetler-Stevenson, M., Yang, J.C., Phan, G.Q., Hughes, M.S., Sherry, R.M., et al. (2015). Chemotherapy-refractory diffuse large B-cell lymphoma and indolent B-cell malignancies can be effectively treated with autologous T cells expressing an anti-CD19 chimeric antigen receptor. J. Clin. Oncol. *33*, 540–549.
9. Porter, D.L., Levine, B.L., Kalos, M., Bagg, A., and June, C.H. (2011). Chimeric antigen receptor-modified T cells in chronic lymphoid leukemia. N. Engl. J. Med. *365*, 725–733.
10. Brentjens, R.J., Davila, M.L., Riviere, I., Park, J., Wang, X., Cowell, L.G., Bartido, S., Stefanski, J., Taylor, C., Olszewska, M., et al. (2013). CD19-targeted T cells rapidly induce molecular remissions in adults with chemotherapy-refractory acute lymphoblastic leukemia. Sci. Transl. Med. *5*, 177ra38.
11. Shah, N.N., Highfill, S.L., Shalabi, H., Yates, B., Jin, J., Wolters, P.L., Ombrello, A., Steinberg, S.M., Martin, S., Delbrook, C., et al. (2020). CD4/CD8 T-Cell Selection Affects Chimeric Antigen Receptor (CAR) T-Cell Potency and Toxicity: Updated Results From a Phase I Anti-CD22 CAR T-Cell Trial. J. Clin. Oncol. *38*, 1938–1950.
12. Ceppi, F., Wilson, A.L., Annesley, C., Kimmerly, G.R., Summers, C., Brand, A., Seidel, K., Wu, Q.V., Beebe, A., Brown, C., et al. (2022). Modified Manufacturing Process Modulates CD19CAR T-cell Engraftment Fitness and Leukemia-Free Survival in Pediatric and Young Adult Subjects. Cancer Immunol. Res. *10*, 856–870.
13. Kochenderfer, J.N., Dudley, M.E., Feldman, S.A., Wilson, W.H., Spaner, D.E., Maric, I., Stetler-Stevenson, M., Phan, G.Q., Hughes, M.S., Sherry, R.M., et al. (2012). B-cell depletion and remissions of malignancy along with cytokine-associated toxicity in a clinical trial of anti-CD19 chimeric-antigen-receptor-transduced T cells. Blood *119*, 2709–2720.
14. Brudno, J.N., Lam, N., Vanasse, D., Shen, Y.W., Rose, J.J., Rossi, J., Xue, A., Bot, A., Scholler, N., Mikkilineni, L., et al. (2020). Safety and feasibility of anti-CD19 CAR T cells with fully human binding domains in patients with B-cell lymphoma. Nat. Med. *26*, 270–280.
15. Song, H.W., Somerville, R.P., Stroncek, D.F., and Highfill, S.L. (2022). Scaling up and scaling out: Advances and challenges in manufacturing engineered T cell therapies. Int. Rev. Immunol. *41*, 638–648.
16. Till, B.G., Jensen, M.C., Wang, J., Chen, E.Y., Wood, B.L., Greisman, H.A., Qian, X., James, S.E., Raubitschek, A., Forman, S.J., et al. (2008). Adoptive immunotherapy for indolent non-Hodgkin lymphoma and mantle cell lymphoma using genetically modified autologous CD20-specific T cells. Blood *112*, 2261–2271.

17. Stroncek, D.F., Ren, J., Lee, D.W., Tran, M., Frodigh, S.E., Sabatino, M., Khuu, H., Merchant, M.S., and Mackall, C.L. (2016). Myeloid cells in peripheral blood mononuclear cell concentrates inhibit the expansion of chimeric antigen receptor T cells. Cytotherapy *18*, 893–901.

18. Deng, B., Pan, J., Liu, Z., Liu, S., Chen, Y., Qu, X., Zhang, Y., Lin, Y., Zhang, Y., Yu, X., et al. (2021). Peripheral leukemia burden at time of apheresis negatively affects the clinical efficacy of CART19 in refractory or relapsed B-ALL. Mol. Ther. Methods Clin. Dev. *23*, 633–643.

19. Neurauter, A.A., Bonyhadi, M., Lien, E., Nøkleby, L., Ruud, E., Camacho, S., and Aarvak, T. (2007). Cell isolation and expansion using Dynabeads. Adv. Biochem. Eng. Biotechnol. *106*, 41–73.

20. Hollyman, D., Stefanski, J., Przybylowski, M., Bartido, S., Borquez-Ojeda, O., Taylor, C., Yeh, R., Capacio, V., Olszewska, M., Hosey, J., et al. (2009). Manufacturing validation of biologically functional T cells targeted to CD19 antigen for autologous adoptive cell therapy. J. Immunother. *32*, 169–180.

21. Priesner, C., Aleksandrova, K., Esser, R., Mockel-Tenbrinck, N., Leise, J., Drechsel, K., Marburger, M., Quaiser, A., Goudeva, L., Arseniev, L., et al. (2016). Automated Enrichment, Transduction, and Expansion of Clinical-Scale CD62L(+) T Cells for Manufacturing of Gene Therapy Medicinal Products. Hum. Gene Ther. *27*, 860–869.

22. Sommermeyer, D., Hudecek, M., Kosasih, P.L., Gogishvili, T., Maloney, D.G., Turtle, C.J., and Riddell, S.R. (2016). Chimeric antigen receptor-modified T cells derived from defined CD8+ and CD4+ subsets confer superior antitumor reactivity in vivo. Leukemia *30*, 492–500.

23. Terakura, S., Yamamoto, T.N., Gardner, R.A., Turtle, C.J., Jensen, M.C., and Riddell, S.R. (2012). Generation of CD19-chimeric antigen receptor modified CD8+ T cells derived from virus-specific central memory T cells. Blood *119*, 72–82.

24. Shalabi, H., Qin, H., Su, A., Yates, B., Wolters, P.L., Steinberg, S.M., Ligon, J.A., Silbert, S., DéDé, K., Benzaoui, M., et al. (2022). CD19/22 CAR T cells in children and young adults with B-ALL: phase 1 results and development of a novel bicistronic CAR. Blood *140*, 451–463.

25. Zhu, F., Shah, N., Xu, H., Schneider, D., Orentas, R., Dropulic, B., Hari, P., and Keever-Taylor, C.A. (2018). Closed-system manufacturing of CD19 and dual-targeted CD20/19 chimeric antigen receptor T cells using the CliniMACS Prodigy device at an academic medical center. Cytotherapy *20*, 394–406.

26. Turtle, C.J., Hanafi, L.A., Berger, C., Gooley, T.A., Cherian, S., Hudecek, M., Sommermeyer, D., Melville, K., Pender, B., Budiarto, T.M., et al. (2016). CD19 CAR-T cells of defined CD4+:CD8+ composition in adult B cell ALL patients. J. Clin. Invest. *126*, 2123–2138.

27. Bernard, F., Jaleco, S., Dardalhon, V., Steinberg, M., Yssel, H., Noraz, N., Taylor, N., and Kinet, S. (2002). Ex vivo isolation protocols differentially affect the phenotype of human CD4+ T cells. J. Immunol. Methods *271*, 99–106.

28. Lyons, P.A., Koukoulaki, M., Hatton, A., Doggett, K., Woffendin, H.B., Chaudhry, A.N., and Smith, K.G.C. (2007). Microarray analysis of human leucocyte subsets: the advantages of positive selection and rapid purification. BMC Genom. *8*, 64.

29. Fry, T.J., Shah, N.N., Orentas, R.J., Stetler-Stevenson, M., Yuan, C.M., Ramakrishna, S., Wolters, P., Martin, S., Delbrook, C., Yates, B., et al. (2018). CD22-targeted CAR T cells induce remission in B-ALL that is naive or resistant to CD19-targeted CAR immunotherapy. Nat. Med. *24*, 20–28.

30. Vantourout, P., and Hayday, A. (2013). Six-of-the-best: unique contributions of γδ T cells to immunology. Nat. Rev. Immunol. *13*, 88–100.

31. Wang, X., Borquez-Ojeda, O., Stefanski, J., Du, F., Qu, J., Chaudhari, J., Thummar, K., Zhu, M., Shen, L.B., Hall, M., et al. (2021). Depletion of high-content CD14(+) cells from apheresis products is critical for successful transduction and expansion of CAR T cells during large-scale cGMP manufacturing. Mol Ther Methods Clin Dev *22*, 377–387.

32. Arcangeli, S., Falcone, L., Camisa, B., De Girardi, F., Biondi, M., Giglio, F., Ciceri, F., Bonini, C., Bondanza, A., and Casucci, M. (2020). Next-Generation Manufacturing Protocols Enriching TSCM CAR T Cells Can Overcome Disease-Specific T Cell Defects in Cancer Patients. Front. Immunol. *11*, 1217.

33. Stanciu, L.A., Shute, J., Holgate, S.T., and Djukanović, R. (1996). Production of IL-8 and IL-4 by positively and negatively selected CD4+ and CD8+ human T cells following a four-step cell separation method including magnetic cell sorting (MACS). J. Immunol. Methods *189*, 107–115.

34. Zhang, D.K.Y., Adu-Berchie, K., Iyer, S., Liu, Y., Cieri, N., Brockman, J.M., Neuberg, D., Wu, C.J., and Mooney, D.J. (2023). Enhancing CAR-T cell functionality in a patient-specific manner. Nat. Commun. *14*, 506.

35. Teachey, D.T., Lacey, S.F., Shaw, P.A., Melenhorst, J.J., Maude, S.L., Frey, N., Pequignot, E., Gonzalez, V.E., Chen, F., Finklestein, J., et al. (2016). Identification of Predictive Biomarkers for Cytokine Release Syndrome after Chimeric Antigen Receptor T-cell Therapy for Acute Lymphoblastic Leukemia. Cancer Discov. *6*, 664–679.

36. Giavridis, T., van der Stegen, S.J.C., Eyquem, J., Hamieh, M., Piersigilli, A., and Sadelain, M. (2018). CAR T cell-induced cytokine release syndrome is mediated by macrophages and abated by IL-1 blockade. Nat. Med. *24*, 731–738.

37. McNerney, K.O., DiNofia, A.M., Teachey, D.T., Grupp, S.A., and Maude, S.L. (2022). Potential Role of IFNγ Inhibition in Refractory Cytokine Release Syndrome Associated with CAR T-cell Therapy. Blood Cancer Discov. *3*, 90–94.

38. Hines, M.R., Keenan, C., Maron Alfaro, G., Cheng, C., Zhou, Y., Sharma, A., Hurley, C., Nichols, K.E., Gottschalk, S., Triplett, B.M., and Talleur, A.C. (2021). Hemophagocytic lymphohistiocytosis-like toxicity (carHLH) after CD19-specific CAR T-cell therapy. Br. J. Haematol. *194*, 701–707.

39. Gentles, A.J., Newman, A.M., Liu, C.L., Bratman, S.V., Feng, W., Kim, D., Nair, V.S., Xu, Y., Khuong, A., Hoang, C.D., et al. (2015). The prognostic landscape of genes and infiltrating immune cells across human cancers. Nat. Med. *21*, 938–945.

40. Capsomidis, A., Benthall, G., Van Acker, H.H., Fisher, J., Kramer, A.M., Abeln, Z., Majani, Y., Gileadi, T., Wallace, R., Gustafsson, K., et al. (2018). Chimeric Antigen Receptor-Engineered Human Gamma Delta T Cells: Enhanced Cytotoxicity with Retention of Cross Presentation. Mol. Ther. *26*, 354–365.

41. Melenhorst, J.J., Chen, G.M., Wang, M., Porter, D.L., Chen, C., Collins, M.A., Gao, P., Bandyopadhyay, S., Sun, H., Zhao, Z., et al. (2022). Decade-long leukaemia remissions with persistence of CD4(+) CAR T cells. Nature *602*, 503–509.

42. Dreyzin, A., Panch, S.R., Shalabi, H., Yates, B., Highfill, S.L., Jin, P., Stroncek, D., and Shah, N.N. (2023). Cryopreserved anti-CD22 and bispecific anti-CD19/22 CAR T cells are as effective as freshly infused cells. Mol. Ther. Methods Clin. Dev. *28*, 51–61.

43. Panch, S.R., Srivastava, S.K., Elavia, N., McManus, A., Liu, S., Jin, P., Highfill, S.L., Li, X., Dagur, P., Kochenderfer, J.N., et al. (2019). Effect of Cryopreservation on Autologous Chimeric Antigen Receptor T Cell Characteristics. Mol. Ther. *27*, 1275–1285.

44. Achar, S.R., Bourassa, F.X.P., Rademaker, T.J., Lee, A., Kondo, T., Salazar-Cavazos, E., Davies, J.S., Taylor, N., François, P., and Altan-Bonnet, G. (2022). Universal antigen encoding of T cell activation from high-dimensional cytokine dynamics. Science *376*, 880–884.

**OMTM, Volume *32***

## Supplemental information

# Manufacture of CD22 CAR T cells following positive versus negative selection results in distinct cytokine secretion profiles and γδ T cell output

**Hannah W. Song, Mehdi Benzaoui, Alka Dwivedi, Sarah Underwood, Lipei Shao, Sooraj Achar, Vesna Posarac, Victoria A. Remley, Michaela Prochazkova, Yihua Cai, Ping Jin, Robert P. Somerville, David F. Stroncek, Grégoire Altan-Bonnet, Nirali N. Shah, Christopher D. Chien, Naomi Taylor, and Steven L. Highfill**

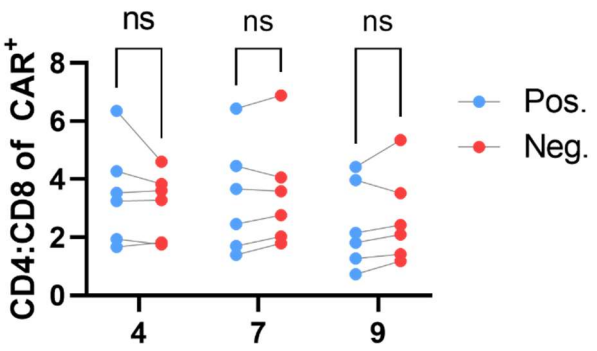


**Figure S1: CD4:CD8 ratio in CAR$^+$ T cells.** The ratio of CD4:CD8 cells was assessed after gating on viable CD3$^+$CAR$^+$ cells at days 4, 7, and 9 following positive and negative selection. ns, non-significant

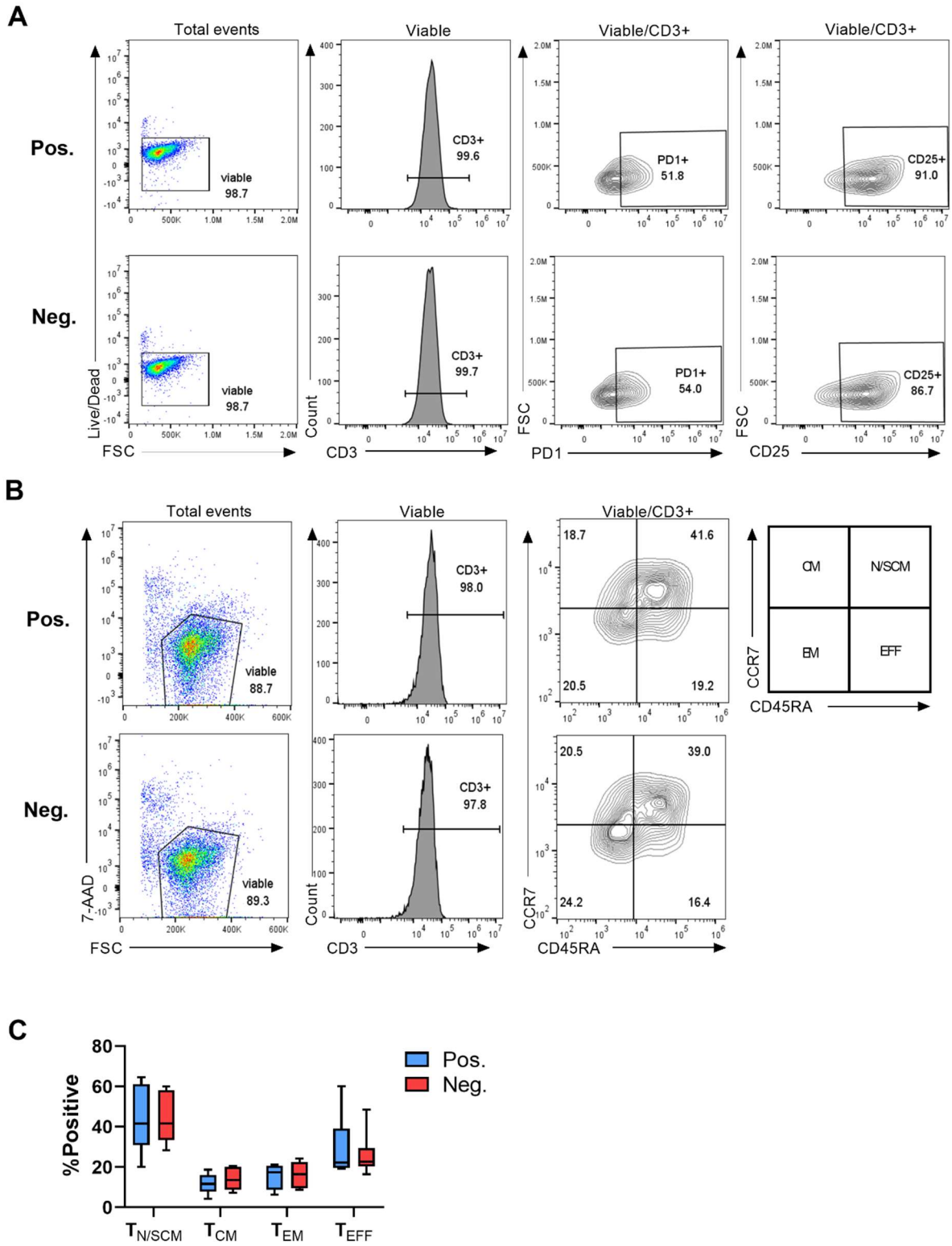


**Figure S2: Representative flow cytometry plots assessing T cell phenotype and activation markers.** (**A**) Representative plots showing the gating of PD-1 and CD25 activation markers on $CD3^+$ T cells at day 9. (**B**) Representative plots showing CD45RA/CCR7 profiles distinguishing naïve/stem cell memory-like (N/SCM), central memory (CM), effector (E), and terminal effector (EFF) T cells at day 9. (C) The percentages of each subset were evaluated on gated $CD3^+$ T cells at Day 9 and means ± SEM (N=6) are shown.

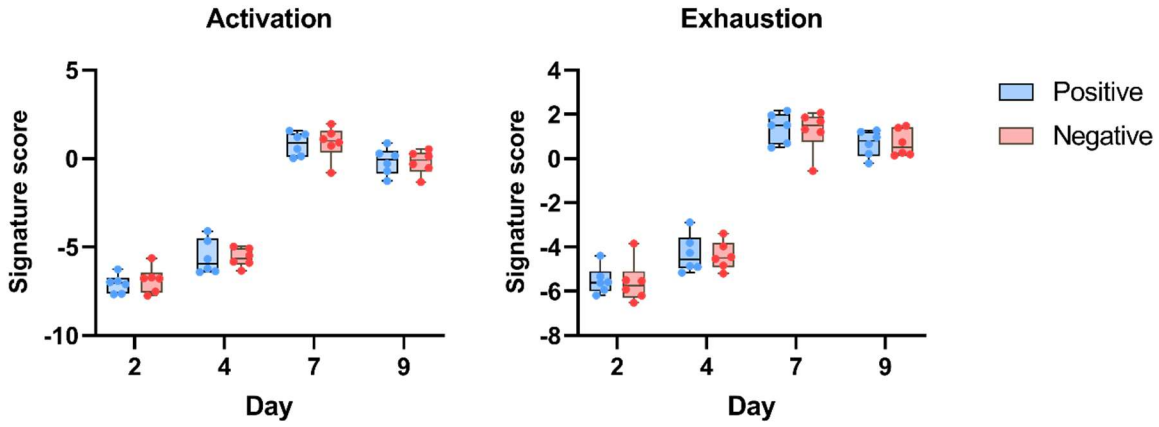


**Figure S3**: **Signature scores of activation and cytotoxicity pathways on negatively-selected and positively-selected T cells.** Pathway analysis of gene expression data for activation and cytotoxicity pathways were assessed at days 2, 4, 7, and 9 of culture. Means ± SEM (n=6 donors) are shown.

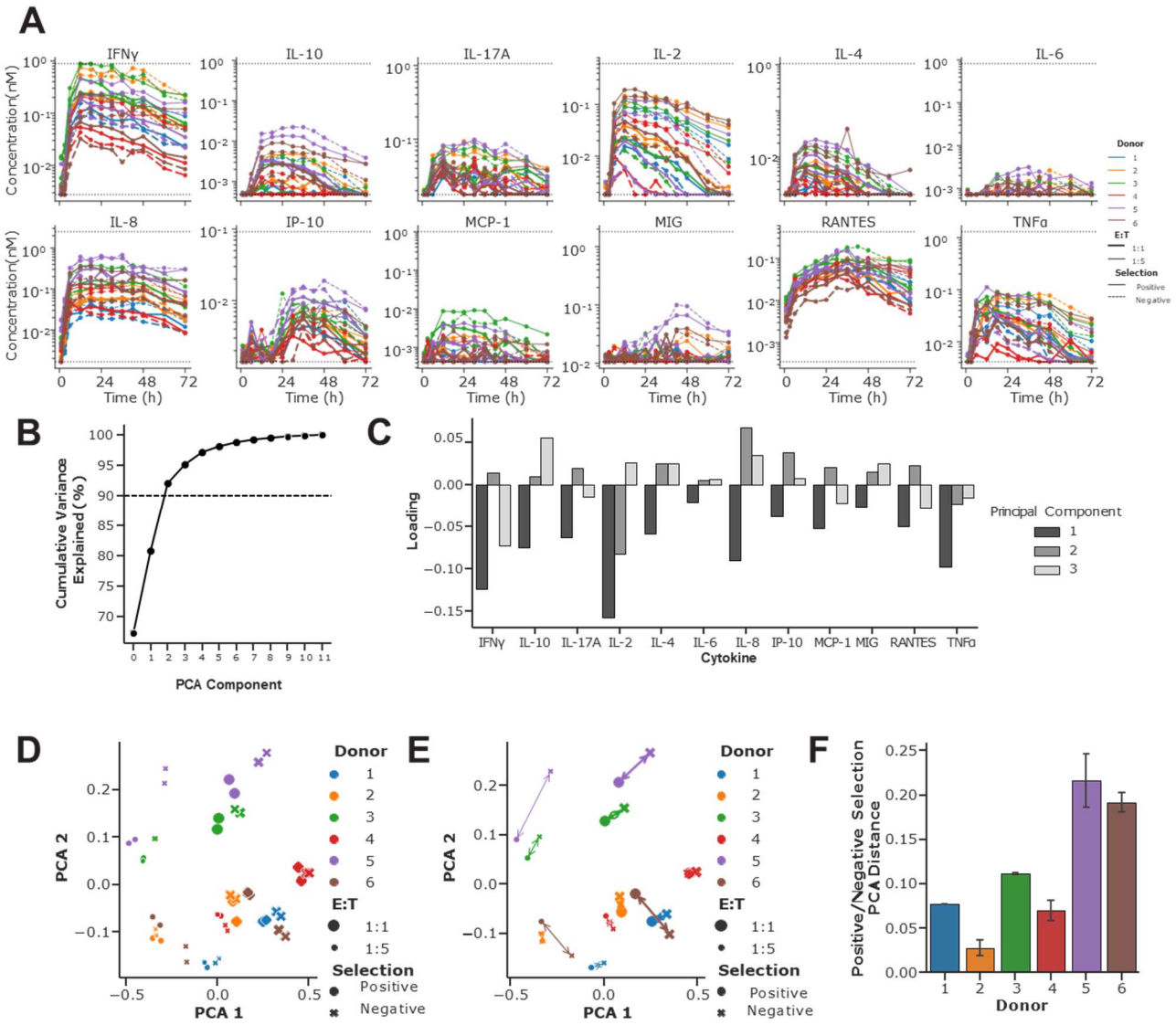


**Figure S4. Dynamics of cytokine secretion by CD22 CART$^{pos}$ and CART$^{neg}$ in response to NALM6 leukemia.** (**A**) Cytokine secretion by CD22 CART generated from 6 donors was evaluated following co-culture with NALM6 at a 1:1 effector/target (E:T) ratio. Cytokines were monitored at 1, 3, 6, 12, 18, 24, 30, 36, 42, 48, 60, and 72h timepoints on a TECAN EVO 100 robotic system. Raw Immunotron cytokine trajectories are shown; dotted lines represent the upper and lower limits of detection for each cytokine. (**B**) Cumulative variance explained for PCA on average cytokine secretion levels per sample; 3 components are sufficient to reach ~90% variance explained. (**C**) Loadings for the first 3 PCA components. (**D**) PCA1/PCA2 profiles of each sample following co-culture with NALM6 leukemia at a 1:1 and 1:5 E/T ratio. (**E**) Distances between positive and negative selections for each set of samples in PCA space. (**F**) PCA distances show considerable heterogeneity between donors, signifying that positive and negative selection had a greater impact on the cytokine secretion of cells derived from some donors over others.

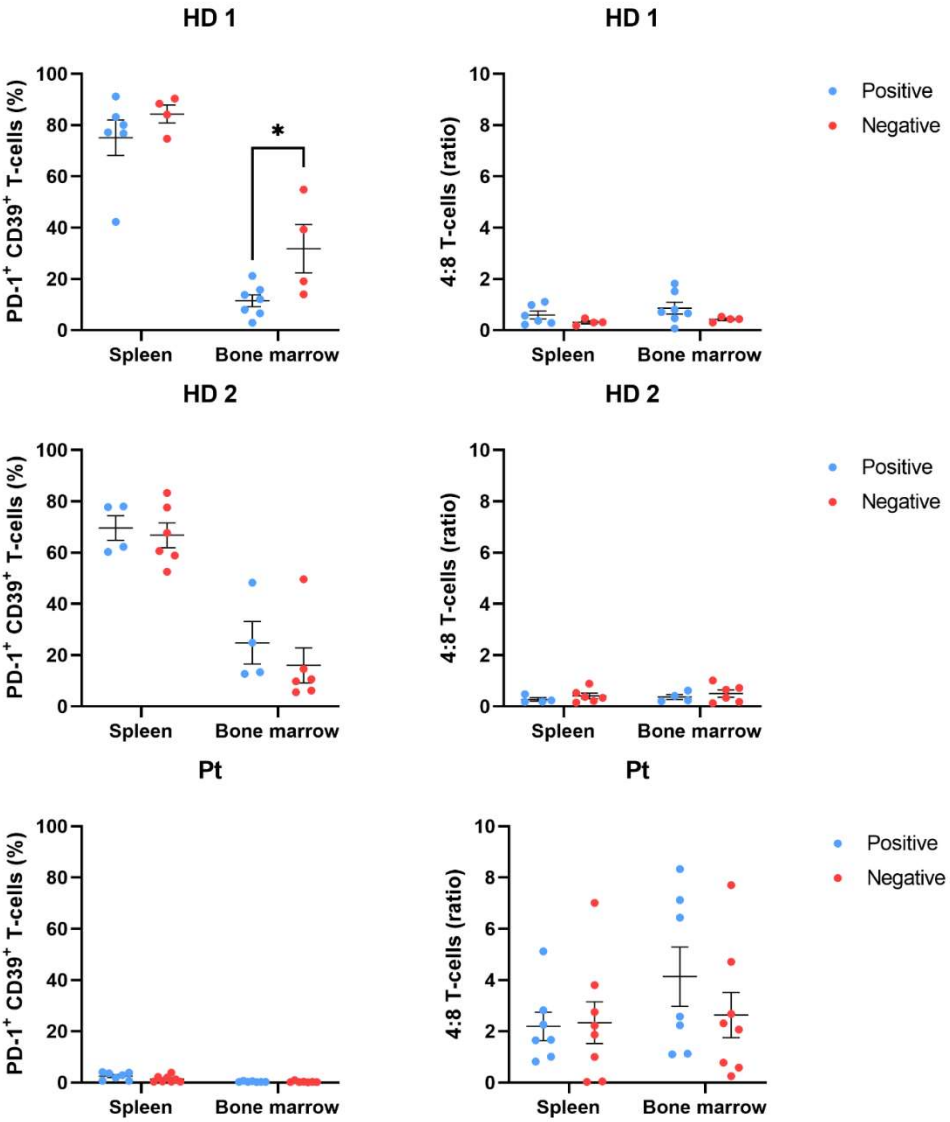


**Figure S5. CD4/CD8 ratios and the PD1$^{+}$CD39$^{+}$ phenotype of CD22 CART persisting in NALM6-bearing NSG mice vary as a function of donor.** Following adoptive transfer of CD22 CART$^{pos}$ and CART$^{neg}$ from 3 donors (HD1, HD2, and Pt) into NSG mice with NALM6 leukemia, mice were sacrificed (day 10) and the phenotypes of human T cells in spleen and bone marrow were evaluated. The percentages of PD1$^{+}$CD39$^{+}$ T cells and their CD4/CD8 profiles were monitored by flow cytometry and a quantification of these cells are shown for each donor (n=4-7 mice per group).

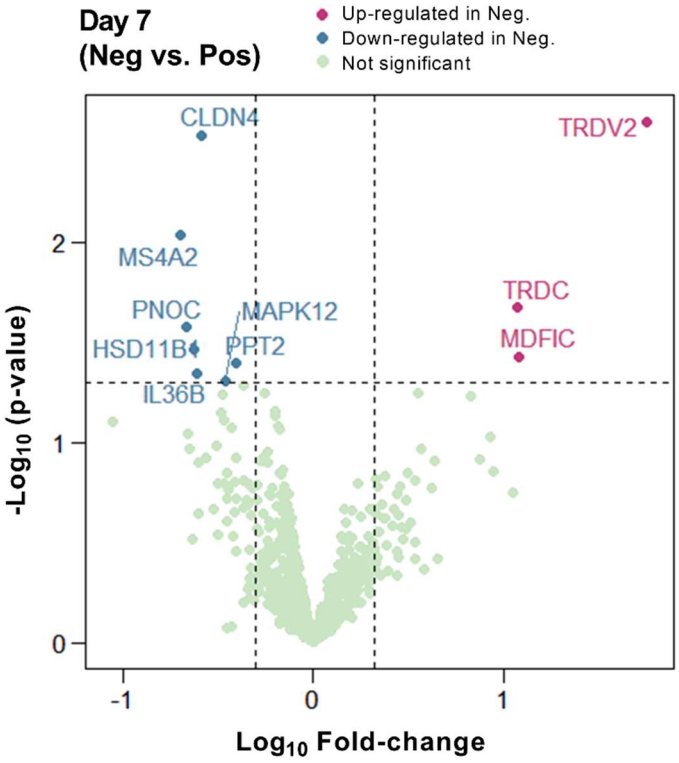


**Figure S6. Differential gene expression in CD22 CART$^{pos}$ and CART$^{neg}$.** Volcano plot representation of differential gene expression between CD22 CART$^{pos}$ and CART$^{neg}$ (day 7 of expansion). Fold changes of >2 and $p<0.05$ were considered significant (dotted lines). The identities of several differentially expressed transcripts are indicated.

**Table S1: Flow cytometry reagents.**

| Marker | Conjugate | Catalog # | Clone | Dilution |
|---|---|---|---|---|
| CCR7 | FITC | BD 561271 | 150503 | 1:100 |
| CD3 | APC-H7 | BD 641397 | SK7 | 1:100 |
| CD3 | BV650 | BD 563999 | SK7 | 1:100 |
| CD4 | BV605 | BD 562658 | RPA-T4 | 1:100 |
| CD4 | AF-700 | BD 557922 | RPA-T4 | 1:100 |
| CD4 | PerCP | BD 344624 | SK3 | 1:100 |
| CD8 | FITC | BD 347313 | SK1 | 1:100 |
| CD8 | BV-510 | BD 563919 | SK1 | 1:100 |
| CD8 | BV605 | BD 300936 | HIT8a | 1:100 |
| CD25 | PE-Cy7 | BD 557741 | M-A251 | 1:100 |
| CD45RA | BV421 | BD 562885 | HI100 | 1:100 |
| CD45RO | BV605 | BD 562791 | UCHL1 | 1:100 |
| CD62L | PE-Cy7 | BD 565535 | DREG56 | 1:100 |
| LAG3 | APC-R700 | BD 565774 | T47-530 | 1:100 |
| PD-1 | BV421 | BD 562516 | EH12.1 | 1:100 |
| Protein L | Biotin | Pierce 29997 | n/a | 20:100 |
| Streptavidin | FITC | Invitrogen S32354 | n/a | 1:100 |
| TCRαβ | PE | Miltenyi 130-113-537 | REA652 | 1:100 |
| TCRVδ1 | APC | Miltenyi 130-118-968 | REA173 | 1:100 |
| TCRVδ2 | BV421 | Miltenyi 130-111-015 | REA771 | 1:100 |
| Viability | Fixable Aqua Dead Cell Stain | Agilent L34966 | n/a | 1:100 |
| Viability | LIVE/DEAD™ Fixable Near-IR Dead Cell Stain | Biolegend L34976A | n/a | 1:100 |
| Viability | 7-AAD | BD 559925 | n/a | 3:100 |